

# Stratospheric aerosol clouds due to very large volcanic eruptions of the early twentieth century: Effective particle sizes and conversion from pyrhelimetric to visual optical depth

Richard B. Stothers

Institute for Space Studies, Goddard Space Flight Center, NASA, New York

**Abstract.** Spectral and pyrhelimetric measurements of atmospheric transmission were made by staff members of the Astrophysical Observatory of the Smithsonian Institution at Washington, D. C., and at Mount Wilson, California, during the years 1901–1920. These valuable data are analyzed here with the help of a new inversion method to derive the effective, or area-weighted, radii of stratospheric aerosols formed after three very large volcanic eruptions in this period. After the great eruptions of Katmai (1912) and Santa Maria (1902),  $r_{\text{eff}}$  remained close to  $0.3 \mu\text{m}$  for at least two years. This near constancy of  $r_{\text{eff}}$  has been duplicated in modern times by the aerosols from El Chichón (1982). Following Ksudach's (1907) eruption,  $r_{\text{eff}}$  grew from  $0.2\text{--}0.3 \mu\text{m}$  to  $0.4\text{--}0.5 \mu\text{m}$  in about 1 year. Pinatubo's (1991) aerosols grew similarly. Generally speaking, the pyrhelimetric optical depth perturbation, as measured for the three early eruptions, is not equal to the visual optical depth perturbation, but in fact the latter is larger by a factor of about 1.6, at least for  $r_{\text{eff}} = 0.25\text{--}0.45 \mu\text{m}$ . Wider physical implications of the present results are discussed.

## 1. Introduction

Little information exists at present on the chemical composition and size distribution of small particles supplied to the atmosphere by volcanic eruptions that occurred before the eruption of Agung in 1963. Several early scientific observations and experiments performed by Brugmans, du Vasquier, and van Swinden on the European mainland in the course of Iceland's 1783 Laki fissure eruption suggested that the widespread ground level dry fog probably consisted in part of sulfuric acid particles [van Swinden, 1785]. Exactly one century later, a whitish haze seen high in the atmosphere after Krakatau's explosive eruption was conjectured by *Kiessling* [1886] to be composed mostly of sulfurous gases, while sulfuric acid itself was mentioned at least once as a possibility [Symons, 1888, p. 416]. But not until *Junge et al.* [1961] directly sampled an apparently permanent stratospheric layer of sulfate aerosols, and *Mossop* [1964] detected a proliferation of these aerosols following Agung's eruption, did the case for sulfuric acid aerosols as the main constituent of volcanic dust veils begin to gain general acceptance. Modern measurements of acidity excesses in the annual layers of ice laid down in polar regions have also strongly supported this conclusion in the case of many early eruptions [Hammer, 1977].

Although it is now safe to presume that aerosols composed of  $\text{H}_2\text{SO}_4$  in a water solution have always predominated in volcanic dust veils, the effective particle radius has undoubtedly varied as much in the case of the older eruptions as it has for modern ones. Ground-based spectral measurements of the direct solar radiation after the 1902 eruption of Santa Maria [Abbot, 1903; Langley, 1903a] and again after the 1912 eruption

of Katmai [Abbot et al., 1913, 1922] revealed that the volcanic aerosol extinction followed a wavelength dependence somewhere between  $\lambda^{-4}$  for Rayleigh scattering and a constant value. This suggested that the modal radius of the dust particles responsible was "much greater" [Abbot et al., 1913] than the radius of ordinary air molecules. More recently, *Deirmendjian* [1973] used his water-haze models to infer a modal value of  $0.07 \mu\text{m}$  from the Katmai data. We will show, however, that this result seriously underestimates the modal radius.

It is now feasible to analyze much more carefully the wavelength-dependent atmospheric transmission data that were published by Abbot et al. for the volcanically disturbed periods following the great eruptions of Santa Maria ( $15^\circ\text{N}$ , October 24, 1902), Ksudach ( $52^\circ\text{N}$ , March 28, 1907), and Katmai ( $58^\circ\text{N}$ , June 6, 1912). Our main objectives here are twofold: first, to infer the effective size of the stratospheric aerosol particles in the months and years after each eruption and, second, to determine the approximate ratio of the visual and pyrhelimetric optical depth perturbations. This ratio,  $k$ , is needed if one wishes to convert the large number of transmission measurements made with pyrhelimeters to a standard visual reference wavelength of  $\lambda = 0.55 \mu\text{m}$ .

## 2. Data and Reduction Methods

In 1901 the Astrophysical Observatory of the Smithsonian Institution (APO) under the direction of S. P. Langley and, later, C. G. Abbot began a program of systematic pyrhelimetric and spectrophotometric observations of the cloud-free Sun that continued in various parts of the world for six decades. The purpose was to determine the solar constant and its possible variations. The history of this program has been sketched by several authors, notably by *Hoyt* [1979].

The part of the program that concerns us here occupied the first two decades, during which occurred the two greatest twen-

This paper is not subject to U.S. copyright. Published in 1997 by the American Geophysical Union.

Paper number 96JD03985.

tieth century eruptions before Agung. In those years the main observing sites were Washington, D. C. (39°N) [Langley, 1903b, 1904; Abbot, 1903; Abbot and Fowle, 1908] and Mount Wilson, California (34°N) [Abbot and Fowle, 1908; Abbot et al., 1913, 1922]. The Washington observations covered the years 1901–1907, and the Mount Wilson ones 1905–1906 and 1908–1920. Two very short series of measurements made at Mount Whitney, California (37°N) in 1909–1910 and at Bassour, Algeria (36°N) in 1912 [Abbot et al., 1913] can be only approximately calibrated and so will not be utilized here. After the great eruptions of 1902 and 1912, Abbe [1904] and Kimball [1913] petitioned astronomers to supply any unpublished extinction measurements of starlight. Unfortunately, the resulting sets of stellar data are of little practical value, being uncalibrated and very crude [Stothers, 1996].

Owing to the humid climate of Washington, D. C., the earliest spectrophotometric observations of the Sun are not of the best quality, and Abbot and Fowle [1908] eventually published a final list of only their most reliable transmission measurements (for 1902–1907) which will necessarily be adopted here. A much larger number of measurements are available for Mount Wilson, and almost all are useful. The only data rejected by us include measurements on the following dates: May 25, 1904 (Washington); June 4, 1908; July 31, 1912 (afternoon); August 8, 1913; September 24, 1913; August 5, 1914; September 3, 1915 ( $\lambda = 1.00 \mu\text{m}$ ); and August 10, 1916. The 1915 entry appears to be a typographical error, while the measured transmission decreases on the other seven dates are several standard deviations away from the running mean. Nevertheless, their omission does not significantly affect our final results, which are based on averages over a large number of days. The Mount Wilson observations span only the months April through November, and do not include all of these months in every year.

All spectrophotometric measurements were obtained with a prism instrument, utilizing many narrow spectral bands. However, Abbot et al. published their final results only for a few selected wavelengths. Since the most abundant published data refer to  $\lambda = 0.35, 0.40, 0.45, 0.50, 0.60, 0.70, 0.80, 1.00, 1.20,$  and  $1.60 \mu\text{m}$ , we will use just these 10 wavelengths. Data are either unavailable or unreliable at some wavelengths shorter than  $0.50 \mu\text{m}$  for some of the years, especially at Washington, D. C. In any case, high absolute accuracy in these ground-based data cannot be expected for the ultraviolet wavelengths,  $\lambda \leq 0.40 \mu\text{m}$  [Abbot et al., 1913; Deirmendjian and Sekera, 1956; Dunkelmann and Skolnik, 1959; Roosen et al., 1973]. Furthermore, some diffuse light inevitably enters the measuring apparatus along with the directly transmitted solar beam and must constitute a growing percentage of the total received flux with decreasing wavelength and with increasing aerosol optical depth. In the case of aerosol optical depths less than 0.3, which are relevant here, this percentage should nevertheless fall under 1% for  $\lambda \geq 0.35 \mu\text{m}$  [Abbot et al., 1932; Sutherland et al., 1975]. To supplement the spectrophotometric measurements, simultaneous pyrheliometric measurements were also made by the APO observers.

Monthly means of the daily direct beam atmospheric transmissions normalized to the zenith have been formed here from the published APO tabular data, just as given. These monthly means are then averaged together to obtain annual means, which are shown in Figure 1 for Washington, and in Figure 2 for Mount Wilson. Notice the abrupt transmission decreases in 1903, 1907 (May), and 1912 due to the three very large volcanic

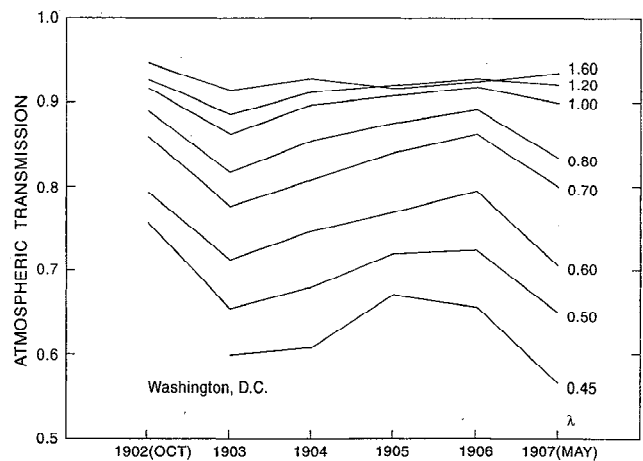


Figure 1. Annual mean atmospheric transmission at Washington, D. C., for eight wavelengths. Not shown is the uncertain transmission at  $\lambda = 0.40 \mu\text{m}$ .

eruptions. After a 2-year period of recovery from the 1912 eruption, another prolonged, but very slight, drop in transmission occurred between 1916 and 1919. This drop may be present also in pyrheliometric measurements made at Uppsala (60°N), Sweden [Volz, 1968], but, elsewhere, it was not systematically or consistently detected. Although Kimball [1916, 1917] and other observers noted some possible independent indications of a weak volcanic disturbance to the atmosphere between July 1916 and early 1917, the effect of the visible haze on atmospheric transmission was essentially negligible [Kimball, 1924], and it did not persist past 1917. On the other hand, D. Hoyt (personal communication, 1996) has pointed out the potential atmospheric effects of large eruptions of Tungurahua (1°S), Ecuador, in 1916 and 1918. Three other large northern hemisphere eruptions also occurred during the period 1917–1919. To be on the safe side, we will adopt as essentially unperturbed years only 1902, 1905, 1906, 1909, 1910, and 1911. Although two Caribbean volcanoes, Soufrière and Pelée, erupted in May 1902, the atmospheric turbidity declined to a fairly small level by October, which is the only month in that year for which useful Washington observations exist [Abbot and Fowle, 1908].

Relative to these assumed normal years, monthly optical depth perturbations,  $\tau_\lambda$ , have been computed by using the following expression derived from Bouguer's law [Stothers, 1996]:

$$\tau_\lambda = \ln [I_N(\lambda)/I_D(\lambda)] \quad (1)$$

where  $I_D$  is the average atmospheric transmission for the volcanically disturbed month and  $I_N$  refers to the same month during unperturbed conditions. In an analogous way, the pyrheliometric extinction,  $\tau_{\text{pyr}}$ , can be computed.

It is important to compare the same months, because  $I_N$  varies slightly from month to month and the variation increases at shorter wavelengths [Roosen et al., 1973]. To illustrate this fluctuation, Figure 3 displays mean monthly transmissions at Mount Wilson for the period 1909–1911. In independent studies of the large optical depth perturbations of July and August 1912, Abbot et al. [1913], Deirmendjian [1973], and Volz [1975] simply compared those two months with the preceding month. Although the optical depth perturbations in 1912 were large enough to minimize any likely incurred error, this would not be

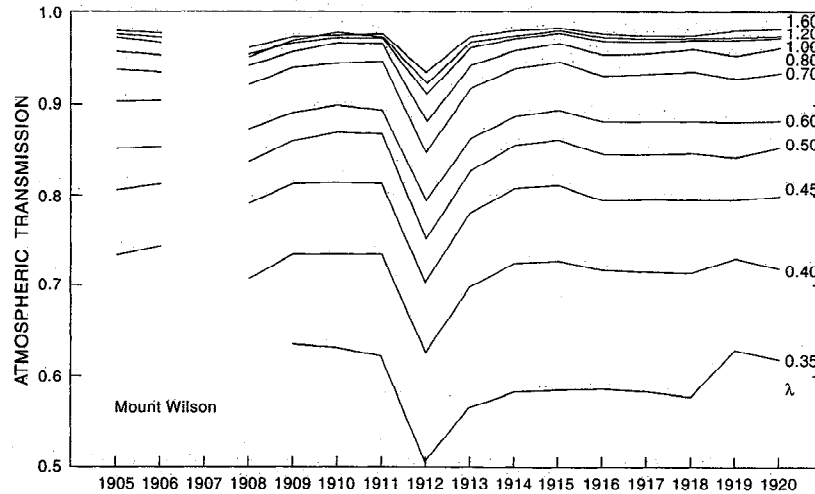


Figure 2. Annual mean atmospheric transmission at Mount Wilson, California, for 10 wavelengths.

true for the smaller optical depth perturbations of other years that are also of interest in the present paper. The only important source of potential error in the reference year method that we have adopted is a possible difference of water vapor content on clear days between perturbed years and unperturbed years. Langley [1904], however, has shown that such differences are negligible even in the highly variable climate of Washington, D. C. This is also true of Mount Wilson [Turco *et al.*, 1982].

A final detail: June 30, 1912, being the first day of the measured high turbidity at Mount Wilson [Abbot *et al.*, 1922], has been grouped with the next month's observing days in forming the July average for that year.

### 3. Wavelength Dependence of Volcanically Produced Extinction

In order to minimize the effects of measurement errors and of day-to-day fluctuations in the observational data, averages over large amounts of data have been taken. This necessitates making a trade-off between high optical depth accuracy and

high time resolution. We have found that the use of annual means of the monthly averages produces the most reliable results from the present data. Accordingly, annual mean optical depth perturbations are plotted as a function of wavelength in Figures 4 and 5 for the volcanically disturbed years 1903–1904 (averaged), 1908, 1912, 1913, and 1914. Data for 1907 are available only for two days in May and therefore are not plotted. However, Table 1 lists these data (showing their scatter) along with the data for the other years. For 1903–1904, only 20 sets of usable daily observations are available over the whole 2-year period, and so a biennial average is necessary. In the four other years, the tabulated annual means are, in reality, summer seasonal means. It is only for the summer of 1912, right after the June 6 eruption of Katmai, that further information might be expected to be gained by treating the July and August data separately. However, individual analyses for the two months yield very similar results (section 4).

Error bars assigned to the optical depths represent  $1\sigma$  standard errors of the annual means. They reflect mostly the large day-to-day turbidity fluctuations throughout the year. Errors in measurement of the daily atmospheric transmissions have been estimated to be only about 2% for both Washington [Abbot,

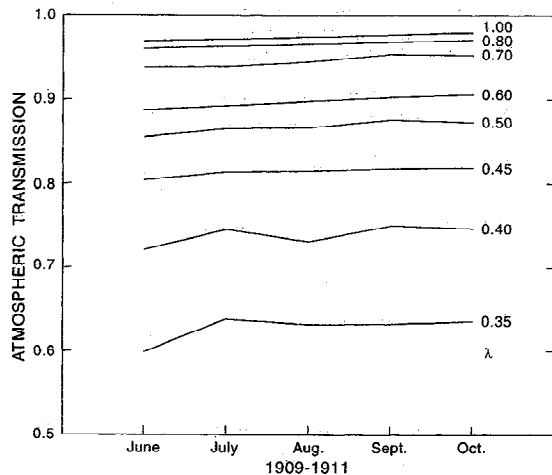


Figure 3. Monthly mean atmospheric transmission at Mount Wilson, California, during the unperturbed period 1909–1911, for eight wavelengths. Curves for  $\lambda = 1.20$  and  $1.60 \mu\text{m}$  are not shown, but are very similar to the curve displayed for  $\lambda = 1.00 \mu\text{m}$ .

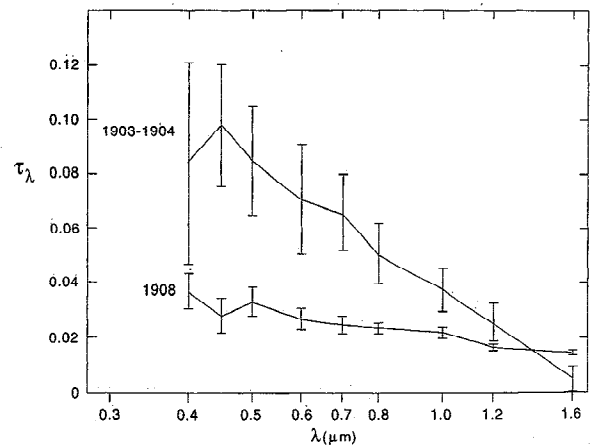
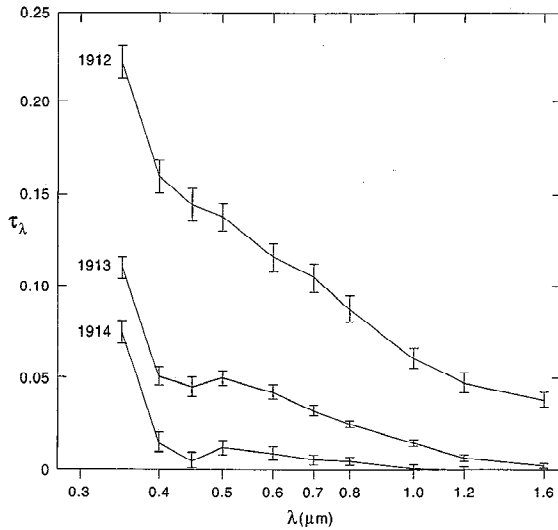


Figure 4. Spectral extinction curves for the optical depth perturbations detected over Washington, D. C., in 1903–1904 and over Mount Wilson, California, in 1908.



**Figure 5.** Spectral extinction curves for the optical depth perturbations detected over Mount Wilson, California, in 1912, 1913, and 1914.

1903] and Mount Wilson [Roosen *et al.*, 1973]. Secular trends of the turbidity also introduce only a minor contribution to the plotted error bars around the annual means.

Shapes of the extinction curves, at least over the wavelength range  $0.40 \leq \lambda \text{ (}\mu\text{m)} \leq 1.60$ , resemble those measured after large volcanic eruptions in modern times, using both Sun and star photometry (see the references cited in section 4). Shortly after the ash phase of a modern eruption, the extinction curve appears quite steep at all wavelengths. But as time progresses it begins to flatten out, starting at the shorter wavelengths. The peculiar sharp rises of the 1912, 1913, and 1914 extinction curves for  $\lambda < 0.40 \mu\text{m}$  are unparalleled in modern experience and therefore are to be doubted as to their physical reality, especially in view of the known uncertainty of the APO measurements for  $\lambda \leq 0.40 \mu\text{m}$  (section 2). These sharp rises will be ignored in what follows.

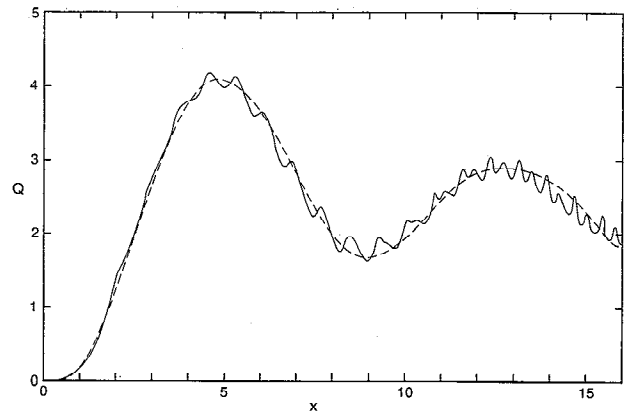


**Figure 6.** Light scattering efficiency factor  $Q$  as a function of size parameter  $x = 2\pi r/\lambda$  for a refractive index  $m = 1.43 - 0i$  (A. Lacis, personal communication, 1996). Dashed curve represents a smooth, eleventh-order polynomial fitted through the eight points:  $x = 0$  (minimum), 1.0, 4.9 (maximum), 7.0, 9.0 (minimum), 12.7 (maximum), 15.0, and 16.0.

#### 4. Effective Particle Sizes

The total aerosol optical thickness of the atmosphere, computed for a column of homogeneous spherical scatterers (Mie particles) in the direction of the zenith, is

$$\tau_\lambda = \int_0^\infty \pi r^2 Q(m, \lambda, r) n(r) H dr. \quad (2)$$

Here  $Q(m, \lambda, r)$  is the light scattering efficiency factor,  $m$  is the complex refractive index of the particles,  $n(r)$  is the average number density of particles with radii between  $r$  and  $r + dr$ , and  $H$  is the total column height. Note that the spectral dependence of  $\tau_\lambda$  arises wholly through  $Q$ , which for an assigned refractive index can be represented uniquely as a function of the size parameter  $x = 2\pi r/\lambda$ . A plot of  $Q$  versus  $x$ , derived in the single-scattering approximation [Hansen and Travis, 1974; also A. Lacis, personal communication, 1996], is shown in Figure 6 for aerosols composed of 75% sulfuric acid

**Table 1.** Wavelength-Dependent Optical Depth Perturbations (Multiplied by 1000) due to the Eruptions of Santa Maria, Ksudach, and Katmai

Year	Month	$N_{\text{obs}}$	Wavelength, $\mu\text{m}$									
			0.35	0.40	0.45	0.50	0.60	0.70	0.80	1.00	1.20	1.60
1903–1904	Jan.–Dec.	20		84	98	85	71	66	51	38	26	5
				37	22	20	20	14	11	8	7	5
1907	May	2		78	163	111	105	63	57	16	2	0
				82	38	28	6	23	17	33	22	49
1908	June–Oct.	97		37	28	33	27	25	24	22	17	15
				6	6	5	4	3	2	2	1	1
1912	July–Aug.	53	223	161	145	138	116	105	88	62	48	39
				9	9	9	8	8	8	7	6	5
1913	Aug.–Oct.	67	110	51	45	50	43	33	25	15	7	3
				6	5	5	4	4	3	2	2	1
1914	June–Oct.	85	74	13	5	12	9	7	5	1	0	0
				6	5	5	4	4	3	2	2	1

$N_{\text{obs}}$  is the number of observations. First row for each year gives the mean optical depth perturbation, while second row gives the standard error of the mean.

**Table 2.** Summary of Spectral Extinction Data and Results of Analysis

Year	Month	$N_{\text{obs}}$	$\tau_{0.55}$	$\tau_{0.80}$	$\tau_{\text{pyr}}$	$\lambda_{\text{pyr}}, \mu\text{m}$	$k$	$\alpha$	$r_{\text{eff}}, \mu\text{m}$
1903–1904	Jan.–Dec.	20	0.078	0.051	0.053	0.78	1.47	1.1	0.31
1907	May	2	0.108	0.057	0.067	0.69	1.61	1.7	0.24
1908	June–Oct.	97	0.030	0.024	0.012 <sup>a</sup>			0.6	0.46
1912	July–Aug.	53	0.127	0.088	0.083	0.84	1.53	1.0	0.33
1913	Aug.–Oct.	67	0.046	0.025	0.028	0.76	1.64	1.6	0.31
1914	June–Oct.	85	0.010	0.005 <sup>b</sup>	0.005 <sup>a</sup>				0.36

<sup>a</sup>Too small to reliably evaluate  $k$ .

<sup>b</sup>Too small to reliably evaluate  $\alpha$ .

and 25% water; the corresponding index of refraction is taken to be  $m = 1.43 - 0i$ . Whatever uncertainty exists concerning the correct value of  $m$  to use will generally lead to very little error in the retrieved values of  $n(r)$  [King *et al.*, 1978].

The simplest case to consider is that of monodisperse, or nearly monodisperse, particles. If  $N$  is the integral of  $n(r)$  over all  $r$ , then

$$\tau_{\lambda} = \pi r^2 Q(m, x) NH. \quad (3)$$

A plot of  $Q$  versus  $x$  thus becomes equivalent to a plot of  $\tau_{\lambda}$  versus  $1/\lambda$ . For small  $x$ ,  $Q$  increases roughly linearly with  $x$ , while for very large  $x$ ,  $Q$  undergoes a damped oscillation, equaling 2 in the mean [Chylek, 1978]. Consequently, at long wavelengths  $\tau_{\lambda}$  varies roughly as  $\lambda^{-1}$ , while at short wavelengths (or for very large particles)  $\tau_{\lambda}$  is nearly independent of  $\lambda$ . The remarkable first maximum of  $Q$  leads to a useful diagnostic for spectral extinction plots: a broad maximum in  $\tau_{\lambda}$ . This maximum peaks at  $\lambda_{\text{max}} \approx 0.55r/(m - 1)$  for  $\text{Im}(m) = 0$  and  $1.33 \leq \text{Re}(m) \leq 1.55$  [van de Hulst, 1957].

In the general case of polydispersions, (2) represents a Fredholm integral equation of the first kind, with a kernel equal to  $\pi^2 QH$ . If complete wavelength information were available, an exact inversion of (2) could be performed to retrieve  $n(r)$ . Since, however, data are available at only a few wavelengths and have large estimated errors, a detailed analysis seems unwarranted; therefore a quick alternative method has been devised here (see the appendix). Specifically,  $Q(x)$  is approximated by a polynomial over a sufficiently large domain of  $x$ , and  $n(r)/N$  is represented by a unimodal lognormal distribution with a modal particle radius  $r_1$  and a geometric standard deviation  $\sigma_1$ . These approximations permit an analytic integration of (2). The resulting theoretical  $\tau_{\lambda}$  curves for different  $(r_1, \sigma_1)$  combinations are then compared with the observations, and the best fit values of  $r_1$  and  $\sigma_1$  follow from a grid search for the smallest residual computed for the various fits. The method has been validated by using a published test case (see the appendix).

Each of the observed  $\tau_{\lambda}$  curves in Figures 4 and 5 yields infinitely many possible solutions, consisting of a continuum of  $(r_1, \sigma_1)$  combinations that produce practically the same effective, or area-weighted, particle radius defined by [van de Hulst, 1957; Hansen and Travis, 1974]

$$r_{\text{eff}} = \int_0^{\infty} r \pi r^2 n(r) dr / \int_0^{\infty} \pi r^2 n(r) dr. \quad (4)$$

For a lognormal distribution, (4) is just

$$r_{\text{eff}} = r_1 \exp[(5/2) \ln^2 \sigma_1]. \quad (5)$$

This indeterminacy regarding  $r_1$  and  $\sigma_1$  arises because the irregularities of the observed  $\tau_{\lambda}$  curves (due to aerosol vari-

ability, measurement errors, data averaging, etc.) lead to about the same rms residual for any smooth fit with just two parameters. Only the effective radius, therefore, is well determined, and hence it alone is entered in Table 2. The theoretical curves, being dependent on  $r_{\text{eff}}$ , are exhibited with the observational points in Figures 7 and 8. If the solutions are redetermined by using different subranges of wavelength, e.g., 0.45–1.2  $\mu\text{m}$ , essentially the same results emerge. For a coarse quantity like  $r_{\text{eff}}$ , it probably matters little in practice (except in pathological cases) whether one mode or several are assumed, or even whether or not the inversion method assumes a specific form for the particle size distribution [Russell *et al.*, 1996].

Over the effective lifetime of Katmai's aerosol cloud, from 1912 to 1914,  $r_{\text{eff}}$  appears to have remained close to 0.3  $\mu\text{m}$ . For Santa Maria, all we can say is that the 2-year (1903–1904) average value of  $r_{\text{eff}}$  was also about 0.3  $\mu\text{m}$ . One year after the eruption of Ksudach (1907), however,  $r_{\text{eff}}$  had increased from an initial value of 0.2–0.3  $\mu\text{m}$  to 0.4–0.5  $\mu\text{m}$ .

These results for Katmai (and probably also for Santa Maria) resemble closely those derived in a similar way for El Chichón, which erupted in March 1982 [King *et al.*, 1984; Spinhirne and King, 1985; Asano *et al.*, 1985; Davies *et al.*, 1988; Brogniez and Lenoble, 1991; Dutton *et al.*, 1994]. Lidar measurements made after El Chichón confirm the extinction-based results [Chazette *et al.*, 1995], and in situ particle counters have also given values of 0.2–0.3  $\mu\text{m}$  [Hofmann and Rosen, 1983, 1984; Knollenberg and Huffman, 1983; Oberbeck *et al.*, 1983; Snetsinger *et al.*, 1987].

In the case of Ksudach, the increase of  $r_{\text{eff}}$  to  $\sim 0.5 \mu\text{m}$  the year after the eruption has been mimicked in the aftermath of

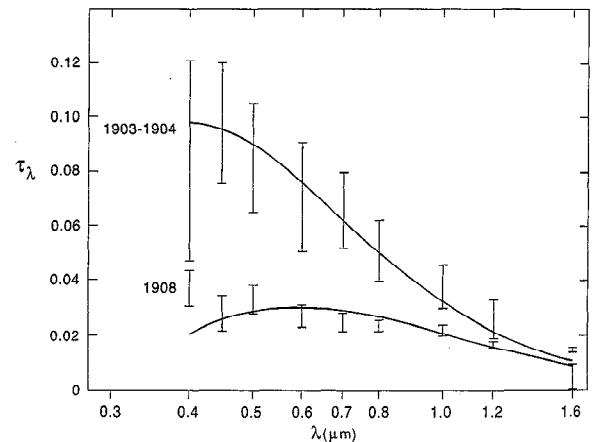


**Figure 7.** Theoretical spectral extinction curves fitted to the optical depth perturbations detected over Washington, D. C., in 1903–1904 and over Mount Wilson, California, in 1908.

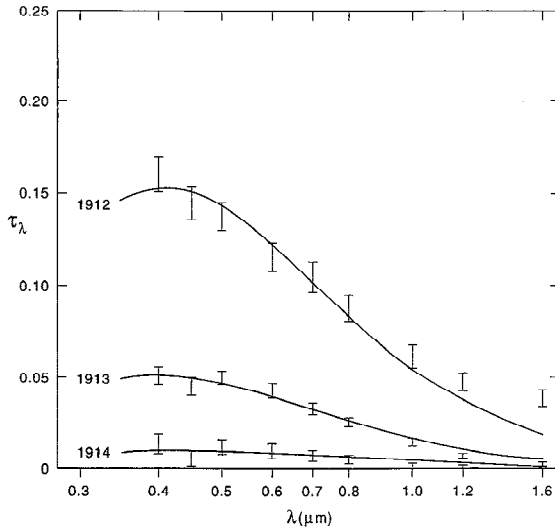


**Figure 8.** Theoretical spectral extinction curves fitted to the optical depth perturbations detected over Mount Wilson, California, in 1912, 1913, and 1914.

Pinatubo's great eruption in June 1991. Effective particle sizes during the period 1991–1994 were derived from spectral extinction measurements [Asano *et al.*, 1993; Stone *et al.*, 1993; Russell *et al.*, 1993, 1996; Pueschel *et al.*, 1994; Dutton *et al.*, 1994; Grainger *et al.*, 1995; Saxena *et al.*, 1995; Herber *et al.*, 1996; Moorthy *et al.*, 1996], lidar measurements [Russell *et al.*, 1993; D'Altorio *et al.*, 1993; Chazette *et al.*, 1995], and in situ particle counts [Deshler *et al.*, 1993; Pueschel *et al.*, 1994; Goodman *et al.*, 1994; Jónsson *et al.*, 1996]. As in the case of El Chichón,  $r_{\text{eff}}$  from particle counts is somewhat smaller than from the other methods.

All these results, however, appear to conflict with the significantly larger particle radii that are implied by the small angular size of Bishop's ring, a diffuse reddish corona that often appears around the Sun after a large volcanic eruption. Bishop's ring showed up after the eruptions of Krakatau, Santa Maria, Ksudach, Katmai, El Chichón, and Pinatubo, as well as after several other modern eruptions. Since the average size of Bishop's ring is virtually an invariant quantity from eruption to eruption [Stothers, 1996] and is presumed to characterize the diffraction pattern produced by nearly monodisperse spherical (Mie) particles, the implied modal particle radius of 0.6–0.8  $\mu\text{m}$  [Symons, 1888; Pernier, 1889; van de Hulst, 1957; Deirmendjian, 1973; Asano, 1993; Sassen *et al.*, 1994] poses a real problem. The phenomenon may imply that the particle size distribution is bimodal or that the conventional interpretations of Bishop's ring are incorrect (work of F. E. Volz, as discussed by van de Hulst [1957]). The slight long-wavelength extinction excess seen in Figure 8, if real, may indicate the presence of a second, large-particle mode during at least the summer of 1912. Such a large-particle mode was occasionally detected with in situ particle counters after the eruptions of El Chichón [Hofmann and Rosen, 1983; Knollenberg and Huffman, 1983; Oberbeck *et al.*, 1983; Snetsinger *et al.*, 1987] and of Pinatubo [Pueschel *et al.*, 1994; Jónsson *et al.*, 1996].

An additional dip in atmospheric transmission at Mount Wilson occurred between mid-July and mid-August 1908. Although comparable in size to two other drops during the same season, and spectrally sloped like a volcanic aerosol curve, this

dip is interesting as having possibly been due to fragments of dust from the Tunguska bolide explosion over Siberia on June 30, 1908 [Fesenkov, 1962; Turco *et al.*, 1982]. On the chance that this was the case, we redid our analysis for 1908, omitting the July and August data. Results are essentially unchanged, as  $r_{\text{eff}}$  increased by only 10%.

## 5. Ratio of Visual to Pyrheliometric Optical Depth

The wavelength at which the spectrally distributed extinction,  $\tau_\lambda$ , equals the pyrheliometric extinction,  $\tau_{\text{pyr}}$ , will be designated  $\lambda_{\text{pyr}}$ . As the slope of the  $\tau_\lambda$  curve steepens,  $\lambda_{\text{pyr}}$  can be expected to drop. Evaluating the Ångström power law exponent,  $\alpha$ , in  $\tau_\lambda \propto \lambda^{-\alpha}$  by a least squares solution over the range  $\lambda = 0.5\text{--}0.8 \mu\text{m}$ , we display the expected drop of  $\lambda_{\text{pyr}}$  in Figure 9 and in Table 2. Notice that  $\lambda_{\text{pyr}}$  does not stray too far above or below a mean value of 0.77  $\mu\text{m}$ , and in fact equals 0.8–0.9  $\mu\text{m}$  for  $\alpha = 1$ , supporting what was previously little more than conjecture [Volz, 1975; Stothers, 1996].

A natural consequence of the decline of  $\lambda_{\text{pyr}}$  with increasing  $\alpha$  is that the ratio,  $k$ , of the visual and pyrheliometric optical depths becomes effectively constant. Averaging the four values derived here for the years 1903–1904, 1907 (May), 1912, and 1913 (all in Table 2), we obtain  $k = 1.56 \pm 0.04$ , confirming preliminary estimates [Volz, 1970, 1975; Stothers, 1996]. This solid result improves on the more commonly adopted assumption  $k = 1$ , valid for a “grey” dust veil [Dyer and Hicks, 1968; Pollack *et al.*, 1976; Bryson and Goodman, 1980; Sato *et al.*, 1993].

Note that  $r_{\text{eff}}$  also declines with increasing  $\alpha$  (Table 2), as would be expected on purely theoretical grounds [Lacis and Mishchenko, 1995].

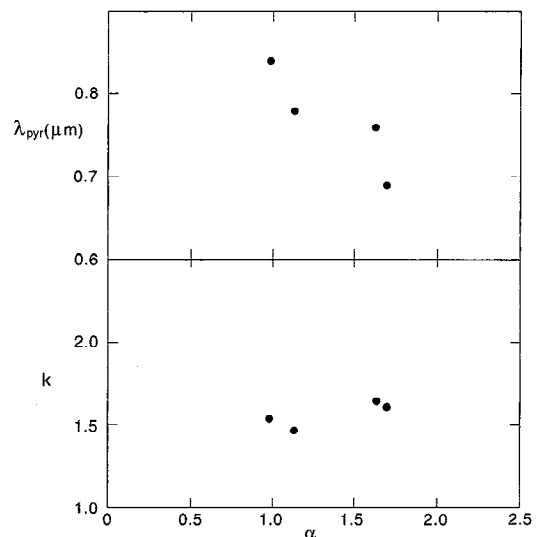


**Figure 9.** Wavelength at which the spectrally distributed extinction equals the pyrheliometric extinction,  $\lambda_{\text{pyr}}$  (upper plot), and the ratio of visual extinction to pyrheliometric extinction,  $k$  (lower plot), as a function of the Ångström power law exponent,  $\alpha$ , in  $\tau_\lambda \propto \lambda^{-\alpha}$ . The cases exhibited refer to the volcanically perturbed years 1903–1904, 1907 (May), 1912, and 1913.

## 6. Conclusion

The APO spectral and pyrheliometric measurements of atmospheric transmission made early in this century retain their usefulness today. The main conclusions derived from the present analysis of them using a new inversion method are as follows:

1. After an initial buildup period of a few weeks, the effective radii of stratospheric aerosols created by the eruptions of Katmai (1912) and Santa Maria (1902) remained close to  $0.3 \mu\text{m}$  for at least 2 years. This near constancy of  $r_{\text{eff}}$  resembles what was observed later after El Chichón (1982). The growth of effective particle radius after Ksudach (1907) to  $0.4\text{--}0.5 \mu\text{m}$  in about 1 year was much like the behavior seen after Pinatubo (1991).

2. Volcanic aerosol extinction as determined from pyrheliometric measurements is found to be equal to the spectrally distributed extinction for a wavelength of  $\lambda_{\text{pyr}} \approx 0.8 \mu\text{m}$ , if  $r_{\text{eff}} \approx 0.3 \mu\text{m}$ .

3. After a large volcanic eruption the visual optical depth perturbation exceeds the pyrheliometric optical depth perturbation by a factor of  $k = 1.6$ , at least if  $r_{\text{eff}} \approx 0.3 \mu\text{m}$ . Although the optical depth perturbation in 1908 was too small for a highly accurate determination of  $k$ , it does suggest  $k = 2.5 \pm 0.8 (1\sigma)$ , which is not significantly different from  $k = 1.6$ .

4. The present results for  $r_{\text{eff}}$  and  $k$  support the previously adopted numerical parameters of a formula that was derived to yield the mass of a volcanic aerosol cloud, given measurements of its pyrheliometric optical depth [Stothers, 1996]. Cloud mass estimates produced in that study are thus confirmed, insofar as they depend on the present evaluation of the microphysical quantities. These results for  $r_{\text{eff}}$  together with the measured optical depths and the observed latitudinal coverage of the aerosol clouds, are nearly all that is needed now to study climate forcing by these clouds [Lacis *et al.*, 1992; Lacis and Mishchenko, 1995].

The number of very large volcanic eruptions about which information on the effective radii of aerosols is available has been approximately doubled by the present study. The two largest recent eruptions have obviously produced very typical aerosols. Indeed, the variation of effective particle radius among all the different eruptions is surprisingly small. This conclusion imposes useful constraints on any chemical and physical processes that may be suggested to build up these aerosols.

## Appendix

Provided that tractable functional forms are adopted as reasonable approximations for  $Q(x)$  and  $n(r)$ , it is possible to integrate the basic equation (2) for  $\tau_\lambda$  analytically. For each assigned refractive index, we represent the exact  $Q(x)$  over the domain  $0 \leq x \leq x_m$  by a polynomial of degree  $I$ :

$$Q(x) = q_1x + q_2x^2 + \cdots + q_Ix^I. \quad (\text{A1})$$

Here  $q_0 = 0$ , because  $Q(0) = 0$ . Although a Lagrange polynomial interpolation formula for a total of  $I$  chosen points might be thought acceptable for finding the coefficients in (A1), that approach usually produces spurious maxima and minima in the fitted approximation to the exact function. Even a polynomial fitted by least squares does not completely solve the difficulty. Therefore we proceed instead by fitting (A1) for  $J$  ( $J < I$ ) points in such a way that the slope at  $I - J$  of these

points is made to be identically zero. These points of zero slope are taken at the major maxima and minima of the exact function (the minor wiggles of the exact function can be ignored). The formal slope equations are

$$0 = q_1 + 2q_2x + \cdots + Iq_Ix^{I-1}. \quad (\text{A2})$$

(A1) and (A2) thus together form a set of  $I$  linear equations, representable in matrix form as

$$\mathbf{Q} = \mathbf{X} \mathbf{q} \quad (\text{A3})$$

where the column vector  $\mathbf{Q}$  has  $J$  elements equal to the chosen  $Q(x)$  values and  $I - J$  elements equal to zero.  $\mathbf{X}$  is a square  $I \times I$  matrix. The solution vector for the unknown  $q_i$  is

$$\mathbf{q} = \mathbf{X}^{-1} \mathbf{Q}. \quad (\text{A4})$$

In practice, points to be fitted are chosen to lie where the exact function has major maxima and minima, with some additional points selected so that, for example, one point might fall on each major rising or declining branch of the exact function. For accuracy, the whole computation should be performed in double-precision arithmetic. A typical fit is shown in Figure 6.

A convenient choice for  $n(r)/N$  is the unimodal lognormal distribution, which often provides a crudely acceptable match to observed stratospheric particle distributions that have been determined from in situ measurements after modern volcanic eruptions:

$$n(r)/N = (2\pi)^{-1/2} (r \ln \sigma_1)^{-1} \cdot \exp \left[ -(\ln r - \ln r_1)^2 / (2 \ln^2 \sigma_1) \right]. \quad (\text{A5})$$

Here  $r_1$  is the mode of the particle radii, and  $\sigma_1$  is the geometric standard deviation. The lognormal distribution possesses the useful property that its moments for  $r$  are separable in  $r_1$  and  $\exp(\ln^2 \sigma_1)$  and contain only simple powers of these quantities:

$$\langle r^n \rangle = \int_0^\infty r^n [n(r)/N] dr = r_1^n \exp \left[ (n^2/2) \ln^2 \sigma_1 \right]. \quad (\text{A6})$$

With these assumptions, (2) integrates to

$$\tau_\lambda = NH \sum_{i=1}^I \pi(2\pi/\lambda)^2 q_i^{i+2} \exp \left[ (i+2)^2 (\ln^2 \sigma_1)/2 \right]. \quad (\text{A7})$$

To infer  $r_1$ ,  $\sigma_1$ , and  $NH$  from observations of  $\tau_\lambda$ , we use the following procedure. With a selected pair of trial values ( $r_1$ ,  $\sigma_1$ ), the above sum is computed for each observed wavelength. Denote the sum  $S(\lambda, r_1, \sigma_1)$ . The formal residual at each wavelength is then computed as the difference between the observed and predicted optical depth perturbations:

$$d(\lambda) = (\tau_\lambda)_{\text{obs}} - S(\lambda, r_1, \sigma_1)NH. \quad (\text{A8})$$

The unknown quantity  $NH$  can be estimated from (A8) by the method of least squares for all  $K$  wavelengths. The rms residual,  $s$ , follows from the computed variance

$$s^2 = \left[ \sum_{k=1}^K d(\lambda_k)^2 \right] / K. \quad (\text{A9})$$

This represents the measure of goodness of fit for each pair of trial values ( $r_1$ ,  $\sigma_1$ ).

It is possible to obtain a complete solution very quickly on a digital computer. For example, the needed powers of the three separate components ( $\lambda$ ,  $r_1$ , and  $\exp(\ln^2 \sigma_1)$ ) appearing in (A7) can be initially computed and stored for all of the observed  $\lambda$  and for all of the assigned trial values of  $r_1$  and  $\sigma_1$ . Subsequently, these stored quantities can be multiplied together as needed to derive all of the sums  $S(\lambda, r_1, \sigma_1)$ . A two-dimensional grid of  $s$  values in  $(r_1, \sigma_1)$  space can be rapidly generated, in which the smallest value of  $s$  indicates the best fit solution. If other trial solutions seem to be nearly as good, this fact can be readily gathered from a glance at the grid. Since, in practice, the inversion of (2) is almost never unique, useful information is obtainable by generating a full grid, a point that has often been ignored in the search for a solution which may actually be only marginally the best fit.

One drawback to the present method is that, to be useful, a high order must be avoided in the polynomial representation of  $Q(x)$ . The formal power series (A1) tends to be of alternating type and approximates the exact function only inside the fitted domain of  $x$ . For  $x > x_m$ , the fitted function diverges positively or negatively depending on the sign of the coefficient of the highest term in the polynomial. If  $I$  is large, the divergence will be very rapid. In the present method, each term in the computed series for  $\tau_\lambda$  also contains a multiplicative factor  $\exp[(i+2)^2(\ln^2 \sigma_1)/2]$ . This factor grows exponentially with increasing  $(i+2)^2$ , restricting the use of the method to moderate values of  $\sigma_1$  in order to avoid a short-wavelength divergence of the computed values of  $\tau_\lambda$ . Such a divergence is caused by the fact that a larger value of  $\sigma_1$  implies the existence of relatively more particles at large radii in the tail of the particle size distribution. If particle numbers do not fall off rapidly enough, any errors in the polynomial representation of  $Q(x)$  at large  $x$  will exert a magnified effect when (2) is integrated over the radius. A test of whether the fitted  $Q(x)$  is adequate or not will be described below.

To check the accuracy of the method, a test case consisting of the inversion of a typical Stratospheric Aerosol and Gas Experiment II (SAGE II) satellite data set was performed. The SAGE II instrument measures aerosol extinction at four wavelengths: 0.385, 0.453, 0.525, and 1.02  $\mu\text{m}$ . The data set used here was obtained on November 30, 1984, and refers to an altitude for the extinction of 19.5 km. This is the data set used by Wang et al. [1989] in an illustration of their method of retrieval of the parameters for an assumed lognormal particle size distribution, based on actual numerical integration of (2) using precise  $Q(x)$  values. Since most of the stratospheric aerosols existing in 1984 had been generated by the eruption of El Chichón in March 1982, Wang et al. adopted a set of wavelength-dependent refractive indices appropriate for sulfuric acid in a cold water solution. We approximate their multiple refractive indices by a single average value,  $m = 1.45 - 0i$ . We also represent  $Q(x)$  by two different polynomials, with even  $I$  and odd  $I$ , in order to verify that the computed  $\tau_\lambda$  values have negligible sensitivity to a negative or positive ultraviolet divergence. Like Wang et al., we find only one true minimum value of the rms residual in  $(r_1, \sigma_1)$  space. Our approximate solution yields  $r_1 = 0.26 \mu\text{m}$  and  $\sigma_1 = 1.28$ , which agrees very well with their more accurate result  $r_1 = 0.25 \mu\text{m}$  and  $\sigma_1 = 1.32$ . Note that the incurred error is considerably smaller than the irreducible uncertainty arising from the SAGE II measurement errors.

In principle, if  $n(r)/N$  were known from accurate in situ particle counts or could be assumed, one might invert (2) to find empirically the wavelength dependence of  $Q(x)$  for sul-

furic acid aerosols. This approach would be analogous to that used in the inversion of observations of solar limb darkening, in which one assumes the radiative source function and empirically infers the wavelength dependence of the extinction (absorption) coefficient for the negative hydrogen ion [Woolley and Stibbs, 1953].

**Acknowledgments.** Useful discussions and correspondence were had with A. A. Lacis, J. E. Hansen, M. I. Mishchenko, F. E. Volz, and D. V. Hoyt. The NASA Climate Research Program provided overall project support.

## References

- Abbe, C., Aufforderung betr. Beobachtungen der Verminderung der Durchsichtigkeit der Erdatmosphäre in den Jahren 1902 und 1903, *Astron. Nachr.*, **165**, 285–288, 1904.
- Abbot, C. G., Recent studies on the solar constant of radiation, *Mon. Weather Rev.*, **31**, 587–592, 1903.
- Abbot, C. G., and F. E. Fowle, Results of "solar-constant" measurements, Mount Wilson and Washington observations, *Ann. Astrophys. Obs. Smithsonian Inst.*, **2**, 96–98, 1908.
- Abbot, C. G., F. E. Fowle, and L. B. Aldrich, *Annals of the Astrophysical Observatory of the Smithsonian Institution*, vol. 3, 241 pp., Smithsonian Inst., Washington, D. C., 1913.
- Abbot, C. G., F. E. Fowle, and L. B. Aldrich, Solar constant and atmospheric transmission at Mount Wilson, 1912 to 1920, *Ann. Astrophys. Obs. Smithsonian Inst.*, **4**, 129–145, 1922.
- Abbot, C. G., L. B. Aldrich, and F. E. Fowle, *Annals of the Astrophysical Observatory of the Smithsonian Institution*, vol. 5, 295 pp., Smithsonian Inst., Washington, D. C., 1932.
- Asano, S., Estimation of the size distribution of Pinatubo volcanic dust from Bishop's ring simulations, *Geophys. Res. Lett.*, **20**, 447–450, 1993.
- Asano, S., M. Sekine, M. Kobayashi, and K. Murai, Atmospheric turbidity and aerosol size distribution in winter at Tsukuba: Effects of the eruption of El Chichon, *J. Meteorol. Soc. Jpn.*, **63**, 453–463, 1985.
- Asano, S., A. Uchiyama, and M. Shiobara, Spectral optical thickness and size distribution of the Pinatubo volcanic aerosols as estimated by ground-based sunphotometry, *J. Meteorol. Soc. Jpn.*, **71**, 165–173, 1993.
- Brognez, C., and J. Lenoble, Analysis of 5-year aerosol data from the Stratospheric Aerosol and Gas Experiment II, *J. Geophys. Res.*, **96**, 15,479–15,497, 1991.
- Bryson, R. A., and B. M. Goodman, Volcanic activity and climatic changes, *Science*, **207**, 1041–1044, 1980.
- Chylek, P., Extinction and liquid water content of fogs and clouds, *J. Atmos. Sci.*, **35**, 296–300, 1978.
- Chazette, P., C. David, J. Lefrère, S. Godin, J. Pelon, and G. Mégie, Comparative lidar study of the optical, geometrical, and dynamical properties of stratospheric postvolcanic aerosols, following the eruptions of El Chichon and Mount Pinatubo, *J. Geophys. Res.*, **100**, 23,195–23,207, 1995.
- D'Altorio, A., F. Masci, V. Rizi, G. Visconti, and M. Verdecchia, Continuous lidar measurements of stratospheric aerosols and ozone after the Pinatubo eruption, 2, Time evolution of ozone profiles and of aerosol properties, *Geophys. Res. Lett.*, **20**, 2869–2872, 1993.
- Davies, J. A., R. Schroeder, and L. J. B. McArthur, Surface-based observations of volcanic aerosol effects, *Tellus*, **40B**, 154–160, 1988.
- Deirmendjian, D., On volcanic and other particulate turbidity anomalies, *Adv. Geophys.*, **16**, 267–296, 1973.
- Deirmendjian, D., and Z. Sekera, Atmospheric turbidity and the transmission of ultraviolet sunlight, *J. Opt. Soc. Am.*, **46**, 565–571, 1956.
- Deshler, T., B. J. Johnson, and W. R. Rozier, Balloonborne measurements of Pinatubo aerosol during 1991 and 1992 at 41°N: Vertical profiles, size distribution, and volatility, *Geophys. Res. Lett.*, **20**, 1435–1438, 1993.
- Dunkelman, L., and R. Skolnik, Solar spectral irradiance and vertical atmospheric attenuation in the visible and ultraviolet, *J. Opt. Soc. Am.*, **49**, 356–367, 1959.
- Dutton, E. G., P. Reddy, S. Ryan, and J. J. DeLuisi, Features and effects of aerosol optical depth observed at Mauna Loa, Hawaii: 1982–1992, *J. Geophys. Res.*, **99**, 8295–8306, 1994.
- Dyer, A. J., and B. B. Hicks, Global spread of volcanic dust from the Bali eruption of 1963, *Q. J. R. Meteorol. Soc.*, **94**, 545–554, 1968.

- Fesenkov, V. G., On the cometary nature of the Tunguska meteorite, *Sov. Astron., Engl. Transl.*, 5, 441–451, 1962.
- Goodman, J., K. G. Snetsinger, R. F. Pueschel, G. V. Ferry, and S. Verma, Evolution of Pinatubo aerosol near 19 km altitude over western North America, *Geophys. Res. Lett.*, 21, 1129–1132, 1994.
- Grainger, R. G., A. Lambert, C. D. Rogers, F. W. Taylor, and T. Deshler, Stratospheric aerosol effective radius, surface area and volume estimated from infrared measurements, *J. Geophys. Res.*, 100, 16,507–16,518, 1995.
- Hammer, C. U., Past volcanism revealed by Greenland ice sheet impurities, *Nature*, 270, 482–486, 1977.
- Hansen, J. E., and L. D. Travis, Light scattering in planetary atmospheres, *Space Sci. Rev.*, 16, 527–610, 1974.
- Herber, A., L. W. Thomason, K. Dethloff, P. Viterbo, V. F. Radionov, and U. Leiterer, Volcanic perturbation of the atmosphere in both polar regions: 1991–1994, *J. Geophys. Res.*, 101, 3921–3928, 1996.
- Hofmann, D. J., and J. M. Rosen, Sulfuric acid droplet formation and growth in the stratosphere after the 1982 eruption of El Chichón, *Science*, 222, 325–327, 1983.
- Hofmann, D. J., and J. M. Rosen, On the temporal variation of stratospheric aerosol size and mass during the first 18 months following the 1982 eruptions of El Chichón, *J. Geophys. Res.*, 89, 4883–4890, 1984.
- Hoyt, D. V., The Smithsonian Astrophysical Observatory solar constant program, *Rev. Geophys.*, 17, 427–458, 1979.
- Jónsson, H. H., J. C. Wilson, C. A. Brock, J. E. Dye, G. V. Ferry, and K. R. Chan, Evolution of the stratospheric aerosol in the northern hemisphere following the June 1991 volcanic eruption of Mount Pinatubo: Role of tropospheric-stratospheric exchange and transport, *J. Geophys. Res.*, 101, 1553–1570, 1996.
- Junge, C. E., C. W. Chagnon, and J. E. Manson, Stratospheric aerosols, *J. Meteorol.*, 18, 81–108, 1961.
- Kiessling, J., Die Bewegung des Krakatau-Rauches im September 1883, *Sitz. König. Preuss. Akad. Wiss.*, 1886(2), 529–533, 1886.
- Kimball, H. H., The effect upon atmospheric transparency of the eruption of Katmai Volcano, *Mon. Weather Rev.*, 41, 153–159, 1913.
- Kimball, H. H., High haze, *Mon. Weather Rev.*, 44, 433–434, 549–550, 1916.
- Kimball, H. H., The smoke cloud and the high haze of 1916, *Mon. Weather Rev.*, 45, 49–52, 1917.
- Kimball, H. H., Variation in solar radiation intensities measured at the surface of the Earth, *Mon. Weather Rev.*, 52, 527–529, 1924.
- King, M. D., D. M. Byrne, B. M. Herman, and J. A. Reagan, Aerosol size distributions obtained by inversion of spectral optical depth measurements, *J. Atmos. Sci.*, 35, 2153–2167, 1978.
- King, M. D., Harshvardhan, and A. Arking, A model of the radiative properties of the El Chichon stratospheric aerosol layer, *J. Clim. Appl. Meteorol.*, 23, 1121–1137, 1984.
- Knollenberg, R. G., and D. Huffman, Measurements of the aerosol size distributions in the El Chichon cloud, *Geophys. Res. Lett.*, 10, 1025–1028, 1983.
- Lacis, A., J. Hansen, and M. Sato, Climate forcing by stratospheric aerosols, *Geophys. Res. Lett.*, 19, 1607–1610, 1992.
- Lacis, A. A., and M. I. Mishchenko, Climate forcing, climate sensitivity and climate response: A radiative modeling perspective on atmospheric aerosols, in *Aerosol Forcing of Climate*, edited by R. J. Charlson and J. Heintzenberg, pp. 11–42, John Wiley, New York, 1995.
- Langley, S. P., Variation of atmospheric absorption, *Nature*, 69, 5, 1903a.
- Langley, S. P., The “solar constant” and related problems, *Astrophys. J.*, 17, 89–99, 1903b.
- Langley, S. P., On a possible variation of the solar radiation and its probable effect on terrestrial temperatures, *Astrophys. J.*, 19, 305–321, 1904.
- Moorthy, K. K., P. R. Nair, B. V. K. Murthy, and S. K. Sathesh, Time evolution of the optical effects and aerosol characteristics of Mt. Pinatubo origin from ground-based observations, *J. Atmos. Terr. Phys.*, 58, 1101–1116, 1996.
- Mossop, S. C., Volcanic dust collected at an altitude of 20 km, *Nature*, 203, 824–827, 1964.
- Oberbeck, V. R., E. F. Danielsen, K. G. Snetsinger, G. V. Ferry, W. Fong, and D. M. Hayes, Effect of the eruption of El Chichon on stratospheric aerosol size and composition, *Geophys. Res. Lett.*, 10, 1021–1024, 1983.
- Pernter, J. M., Der Krakatau-Ausbruch und seine Folge-Erscheinungen, *Meteorol. Z.*, 6, 447–466, 1889.
- Pollack, J. B., O. B. Toon, C. Sagan, A. Summers, B. Baldwin, and W. Van Camp, Volcanic explosions and climate change: A theoretical assessment, *J. Geophys. Res.*, 81, 1071–1083, 1976.
- Pueschel, R. F., P. B. Russell, D. A. Allen, G. V. Ferry, K. G. Snetsinger, J. M. Livingston, and S. Verma, Physical and optical properties of the Pinatubo volcanic aerosol: Aircraft observations with impactors and a Sun-tracking photometer, *J. Geophys. Res.*, 99, 12,915–12,922, 1994.
- Roosen, R. G., R. J. Angione, and C. H. Klemcke, Worldwide variations in atmospheric transmission, 1, Baseline results from Smithsonian observations, *Bull. Am. Meteorol. Soc.*, 54, 307–316, 1973.
- Russell, P. B., et al., Pinatubo and pre-Pinatubo optical-depth spectra: Mauna Loa measurements, comparisons, inferred particle size distributions, radiative effects, and relationship to lidar data, *J. Geophys. Res.*, 98, 22,969–22,985, 1993.
- Russell, P. B., et al., Global to microscale evolution of the Pinatubo volcanic aerosol, derived from diverse measurements and analyses, *J. Geophys. Res.*, 101, 18,745–18,763, 1996.
- Sassen, K., T. Peter, B. P. Luo, and P. J. Crutzen, Volcanic Bishop's ring: Evidence for a sulfuric acid tetrahydrate particle aureole, *Appl. Opt.*, 33, 4602–4606, 1994.
- Sato, M., J. E. Hansen, M. P. McCormick, and J. B. Pollack, Stratospheric aerosol optical depths, 1850–1990, *J. Geophys. Res.*, 98, 22,987–22,994, 1993.
- Saxena, V. K., J. Anderson, and N.-H. Lin, Changes in Antarctic stratospheric aerosol characteristics due to volcanic eruptions as monitored by the Stratospheric Aerosol and Gas Experiment II satellite, *J. Geophys. Res.*, 100, 16,735–16,751, 1995.
- Snetsinger, K. G., G. V. Ferry, P. B. Russell, R. F. Pueschel, V. R. Oberbeck, D. M. Hayes, and W. Fong, Effects of El Chichón on stratospheric aerosols late 1982 to early 1984, *J. Geophys. Res.*, 92, 14,761–14,771, 1987.
- Spinhirne, J. D., and M. D. King, Latitudinal variation of spectral optical thickness and columnar size distribution of the El Chichon stratospheric aerosol layer, *J. Geophys. Res.*, 90, 10,607–10,619, 1985.
- Stone, R. S., J. R. Key, and E. G. Dutton, Properties and decay of stratospheric aerosols in the Arctic following the 1991 eruptions of Mount Pinatubo, *Geophys. Res. Lett.*, 20, 2359–2362, 1993.
- Stothers, R. B., Major optical depth perturbations to the stratosphere from volcanic eruptions: Pyrheliometric period, 1881–1960, *J. Geophys. Res.*, 101, 3901–3920, 1996.
- Sutherland, R. A., R. D. McPeters, G. B. Findley, and A. E. S. Green, Sun photometry and spectral radiometry at wavelengths less than 360 nm, *J. Atmos. Sci.*, 32, 427–436, 1975.
- Symons, G. J., *The Eruption of Krakatoa and Subsequent Phenomena*, Trübner, London, 1888.
- Turco, R. P., O. B. Toon, C. Park, R. C. Whitten, J. B. Pollack, and P. Noerdlinger, An analysis of the physical, chemical, optical, and historical impacts of the 1908 Tunguska meteor fall, *Icarus*, 50, 1–52, 1982.
- van de Hulst, H. C., *Light Scattering by Small Particles*, John Wiley, New York, 1957.
- van Swinden, J. H., Observaciones nebulam, quae mense Junio 1783 apparuit, spectantes, in *Ephemerides Societatis Meteorologicae Palatinae, Observations Anni 1783*, edited by J. Hemmer, pp. 679–688, Schwan, Mannheim, 1785.
- Volz, F. E., Turbidity at Uppsala from 1909 to 1922 from Sjöström's solar radiation measurements, *Medd. Sver. Meteorol. Hydrolog. Inst., Ser. B*, 28, 100–104, 1968.
- Volz, F. E., Atmospheric turbidity after the Agung eruption of 1963 and size distribution of the volcanic aerosol, *J. Geophys. Res.*, 75, 5185–5193, 1970.
- Volz, F. E., Distribution of turbidity after the 1912 Katmai eruption in Alaska, *J. Geophys. Res.*, 80, 2643–2648, 1975.
- Wang, P.-H., M. P. McCormick, T. J. Swissler, M. T. Osborn, W. H. Fuller, and G. K. Yue, Inference of stratospheric aerosol composition and size distribution from SAGE II satellite measurements, *J. Geophys. Res.*, 94, 8435–8446, 1989.
- Woolley, R. v. d. R., and D. W. N. Stibbs, *The Outer Layers of a Star*, chap. 5, Clarendon, Oxford, England, 1953.

R. B. Stothers, Goddard Institute for Space Studies, NASA, 2880 Broadway, New York, NY 10025. (e-mail: asrbs@giss.nasa.gov)

(Received June 25, 1996; revised December 18, 1996; accepted December 18, 1996.)